THEORY OF FERROMAGNETIC MICROSWIMMERS

by Andrew D. Gilbert

(*Mathematics Research Institute,*
College of Engineering, Mathematics and Physical Sciences,
University of Exeter, U.K.)

Feodor Y. Ogrin, Peter G. Petrov and C. Peter Winlove

(*School of Physics,*
College of Engineering, Mathematics and Physical Sciences,
University of Exeter, U.K.)

[Received ?? Revise ??]

Summary

This paper considers the dynamics of a microscale swimmer based on two magnetic beads that are elastically coupled together. A time-varying external magnetic field is imposed that has two principal effects: one is to exert a torque on the magnetic beads. The second is to change the orientation of the magnetic field dipoles in one or both beads, depending on their ferromagnetic properties. This then creates an attraction or repulsion between the two dipoles. The combination of dipole attraction/repulsion, moderated by the elastic coupling, and torque gives motions that are not generally time-reversible and can lead to unidirectional swimming, that is persistent motion in one direction, in a Stokes flow regime.

The equations of motion for the swimmer are set up using a Lagrangian formulation and supplemented by equations giving the dipole orientation of the magnetic fields of the beads in the external field. The equations are non-dimensionalised and key parameters determined. Numerical simulations reveal a number of regimes which are studied using simplified models and multiple scale analysis. Approximate thresholds are obtained above which the swimmer moves in a closed path, and below which the orientation is 'trapped' giving unidirectional motion. Three mechanisms for such trapping are isolated and discussed.

1. Introduction

The problem of how living organisms propel themselves through a fluid such as air or water has a long history [1; 2; 3; 4; 5]. On the small scales of microorganisms, the Reynolds number is very low and swimming occurs in a Stokes flow regime, with negligible inertia. In this regime persistent motion of an organism requires symmetry breaking. If the configuration of a would-be swimmer has a sequence of states that is invariant under time-reversal, then persistent motion through the fluid will not occur. This is true no matter what the time-dependence of the path through the states, since time derivatives do not enter the equations for Stokes flow. This celebrated result of Purcell [6], his 'scallop theorem', has led to study of how microorganisms achieve symmetry breaking and propulsion by mechanisms such as arrays of cilia and rotating flagella; see [7].

More recently there has been much interest in fabricating microscale swimmers and related devices, eventually aimed at functions such as targetted drug delivery or stirring and pumping in microfluidic systems. Microscale swimmers must again break the time-reversal symmetry [6]. A number of models are based on three coupled spherical beads which move relative to each other with a suitable time-irreversible protocol [8; 9; 10; 11] and have been studied together with issues such as swimmer–swimmer interaction and scattering [12; 13]. A general discussion of how swimming is generated by forces and torques on two or more beads is given in [14; 15; 16]. In terms of practically realisable artificial swimmers, one attractive way to drive motions on small scales is by the use of external magnetic fields, whose time-dependence can be specified. A microscale swimmer can then be made up from magnetic beads coupled elastically. These ideas have been used in the fabrication of swimming devices in the form of chains of magnetic beads coupled by flexible links [17; 18], with associated theoretical and numerical models [19; 20; 21].

One of the simplest magnetically based swimming devices realised in the laboratory consists of two ferromagnetic beads joined by an elastic element which could be a vesicle, polymer or protein fibre [22]: the elastic element could also be the component to be transported in a possible medical application. Rotational motion is driven by the torque from an external field. At the same time the direction of the external field and the magnetic anisotropy of the particles influences the directions of the individual ferromagnetic or 'soft' magnets and the dipole force between them, driving a radial component of motion. These two components can result in a range of behaviours in the experiments, including tumbling motion and persistent unidirectional swimming. The aim of the present paper is to give some theoretical underpinning for this experimental model, based on an analysis of motion in a Stokes regime. The leading order effect of the fluid is a Stokes drag on the two magnetic beads, but this alone will not give persistent motion, as the centre of reaction of the swimmer will remain fixed [23; 24; 25]. Instead a fluid interaction term has to be included to obtain persistent swimming: motion of one bead will drive a motion of the other, through the flow of intervening fluid.

In the present paper we set up a model for the ferromagnetic swimmer of [22], our objective being to understand the different regimes of motion, parameters and mechanisms. The key question is: when does the swimmer move persistently in a single direction, unidirectional motion, and when does it simply describe a closed path (perhaps on a large scale) in two dimensions? To investigate this we set up ODEs based on a Lagrangian formulation [24] which include the internal dynamics of the swimmer, that is the distance s between the two magnetic particles or beads and an angle coordinate ϕ, together with the equation for the centre of reaction $\boldsymbol{X}$ driven only by fluid interaction terms. This is supplemented by equations for the directions α_j of the dipoles in each ferromagnetic bead. Simulations of the system show the importance of finding regimes where the angle ϕ is 'trapped' and does not show a persistent, secular drift, otherwise the swimmer moves in a closed path. We then take apart the system of ODEs, simplifying it radically to investigate mechanisms for trapping and the resulting swimmer velocities and behaviours.

We should stress that our philosophy is not primarily to model the swimmer quantitatively: we neglect a number of effects that could play a role in the actual experimental realisation, for example bending of the elastic filament and viscous interactions between the filament and the beads. Our aim rather is to study a minimal model and so to discover relevant parameters and qualitative behaviour in different regimes. For example, a key question is: in which direction does the swimmer move? We use standard multiple scales analysis to probe the ranges of behaviour, and also as a check on simulations. This analysis is based on the smallness of a parameter A and even though it is not so small for our reference simulation (parameters given in table 1 below) the asymptotic results give a good guide to the behaviour we see, as well as showing good agreement for other simulations in the appropriate asymptotic limits of small A. In order to try to crystallise

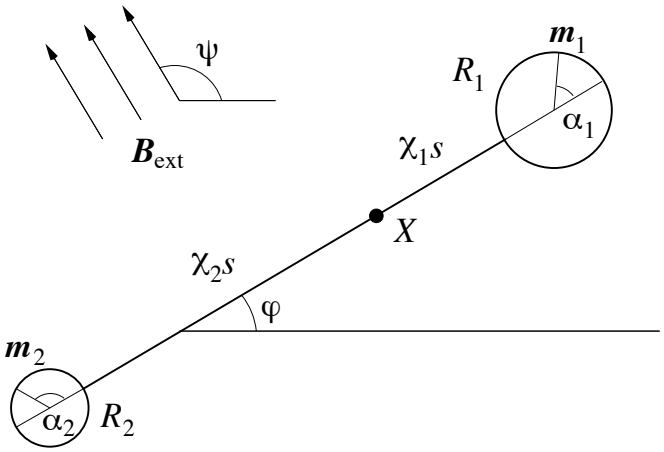

Fig. 1 Coordinate system and geometry of the swimmer.

our results in a useful format, we have set down a number of 'rules of thumb' : these cannot be considered hard and fast but should give guidance in the design and interpretation of future experimental studies.

2. Governing equations

In this section we set out the equations of motion for the swimmer, including inertia and magnetic effects, and non-dimensionalise them. We use a standard Lagrangian formulation as outlined by [24], supplemented by equations giving the orientation of the dipole magnetic fields in the beads. These dipoles relax to orientations depending on the external field and the hardness or softness of the magnets, on a rapid magnetic time scale, much faster than the dynamical time scale of the swimmer or the characteristic time-scale of the external magnetic field.

2.1 *Geometry and Lagrangian formulation*

The geometry we consider is shown in figure 1: the swimmer consists of two elastically coupled magnetic particles or beads, which are labelled by $j = 1$ and $j = 2$ and have radii R_j. We use a Lagrangian formulation, with generalised coordinates $\boldsymbol{q} = (X, Y, s, \phi)$. The distance between the particles is s and the angle made by the line joining the particles to some given x-axis is ϕ. We take the point $\boldsymbol{X} = (X, Y)$ to lie at the centre of reaction [23][†] of the beads, whose positions $\boldsymbol{r}_j$ are then given by

$$\boldsymbol{r}_1 = \boldsymbol{X} + \chi_1 s\hat{\boldsymbol{r}}, \quad \boldsymbol{r}_2 = \boldsymbol{X} - \chi_2 s\hat{\boldsymbol{r}}, \tag{2.1}$$

and velocities by

$$\dot{\boldsymbol{r}}_1 = \dot{\boldsymbol{X}} + \chi_1(\dot{s}\hat{\boldsymbol{r}} + s\dot{\phi}\hat{\boldsymbol{\phi}}), \quad \dot{\boldsymbol{r}}_2 = \dot{\boldsymbol{X}} - \chi_2(\dot{s}\hat{\boldsymbol{r}} + s\dot{\phi}\hat{\boldsymbol{\phi}}). \tag{2.2}$$

[†] See section 5.6 of this reference and note that for simplicity we have taken $\boldsymbol{X}$ as it is defined in the limit $R_j/l_0 \ll 1$, rather than include a correction from fluid interactions.

Here the constants that define $\boldsymbol{X}$ as the centre of reaction are

$$\chi_1 = R_2/(R_1+R_2), \quad \chi_2 = R_1/(R_1+R_2), \tag{2.3}$$

and we define unit vectors $\hat{\boldsymbol{r}} = (\cos\phi, \sin\phi)$, and $\hat{\boldsymbol{\phi}} = (-\sin\phi, \cos\phi)$ with respect to Cartesian axes (x, y). In this paper we work in two dimensions, so the swimmer is assumed to be constrained to a plane, for example by surface tension forces.

The Lagrangian contains all the conservative forces and takes the form

$$L = T - V_{\text{spring}} - V_{\text{mag}} - V_{\text{ext}}. \tag{2.4}$$

Although we will ultimately work in a Stokes regime, at this point we include the kinetic energy so we can assess the magnitude of bead inertia, given by

$$T = \tfrac{1}{2}(\nu_1+\nu_2)\dot{\boldsymbol{X}}^2 + \tfrac{1}{2}(\nu_1\chi_1+\nu_2\chi_2)(\dot{s}^2 + s^2\dot{\phi}^2) + (\nu_1\chi_1 - \nu_2\chi_2)(\dot{s}\hat{\boldsymbol{r}} + s\dot{\phi}\hat{\boldsymbol{\phi}})\cdot\dot{\boldsymbol{X}}, \tag{2.5}$$

where ν_j are the masses of the two particles. Note that to capture all leading order inertial effects quantitatively, the added mass of the fluid would also have to be incorporated, but we do not do this here.

The elastic energy of the filament gives a potential

$$V_{\text{spring}} = \tfrac{1}{2}k(s-l_0)^2, \tag{2.6}$$

where l_0 is the filament's natural length and k is a spring constant. The force between the two magnetic beads corresponds to a potential energy

$$V_{\text{mag}} = \frac{\mu_0}{4\pi s^3}\left[\boldsymbol{m}_1\cdot\boldsymbol{m}_2 - 3(\boldsymbol{m}_1\cdot\hat{\boldsymbol{r}})(\boldsymbol{m}_2\cdot\hat{\boldsymbol{r}})\right] = \frac{\mu_0 m_1 m_2}{4\pi s^3}\left[\cos(\alpha_2-\alpha_1) - 3\cos\alpha_1\cos\alpha_2\right], \tag{2.7}$$

where $\boldsymbol{m}_j$ are the dipole magnetisation vectors which lie at angles α_j to the line joining the particles, as depicted in figure 1. The external magnetic field $\boldsymbol{B}_{\text{ext}}$ drives the swimmer directly through a potential term,

$$V_{\text{ext}} = -\boldsymbol{m}_1\cdot\boldsymbol{B}_{\text{ext}} - \boldsymbol{m}_2\cdot\boldsymbol{B}_{\text{ext}} = -B_{\text{ext}}b[m_1\cos(\phi+\alpha_1-\psi) + m_2\cos(\phi+\alpha_2-\psi)], \tag{2.8}$$

where

$$\boldsymbol{B}_{\text{ext}} = B_{\text{ext}}(b_x, b_y), \quad b_x = b\cos\psi, \quad b_y = b\sin\psi. \tag{2.9}$$

Here we have taken the external field to have scale B_{ext}, for example given by the maximum magnitude of the field over one cycle, and to have phase $\psi(\omega t)$ and dimensionless amplitude $b(\omega t)$, both periodic with period $2\pi/\omega$. Note that at this point, as we treat the magnetic dipole directions outside the Lagrangian framework, the directions $\alpha_j(t)$ are taken as external inputs to the dynamics.

We now include the non-conservative effects of Stokes drag and fluid interactions as generalised forces. Recall that in the Lagragian formulation with generalised coordinates $\boldsymbol{q}$ and Lagrangian $L(\boldsymbol{q}, \dot{\boldsymbol{q}}, t)$, the equations of motion are

$$p_i = \frac{\partial L}{\partial \dot{q}_i}, \quad \dot{p}_i - \frac{\partial L}{\partial q_i} = Q_i, \quad Q_i = \sum_j \boldsymbol{F}_j\cdot\frac{\partial \boldsymbol{r}_j}{\partial q_i}\,. \tag{2.10}$$

Here p_i are generalised momenta and Q_i are generalised forces arising from the dissipative drag forces $\boldsymbol{F}_j$ from the fluid on the two particles $j = 1, 2$. We have coordinates $\boldsymbol{q} = (\boldsymbol{X}, s, \phi)$ and so

$$\boldsymbol{Q} = \boldsymbol{F}_1 + \boldsymbol{F}_2, \quad Q_s = (\chi_1\boldsymbol{F}_1 - \chi_2\boldsymbol{F}_2)\cdot\hat{\boldsymbol{r}}, \quad Q_\phi = (\chi_1\boldsymbol{F}_1 - \chi_2\boldsymbol{F}_2)\cdot s\hat{\boldsymbol{\phi}}. \tag{2.11}$$

Provided the radii $R_j \ll l_0$, the length of the connecting filament, we may write the forces $\boldsymbol{F}_j$ as expansions that include Stokes drag and the leading order fluid interaction term [e.g., 23; 26].

$$\boldsymbol{F}_1 = -6\pi\eta R_1 \dot{\boldsymbol{r}}_1 + \frac{9\pi}{2}\frac{\eta R_1 R_2}{s}(\hat{\boldsymbol{r}}\hat{\boldsymbol{r}} + I)\cdot\dot{\boldsymbol{r}}_2 + \cdots, \tag{2.12}$$

and similarly under interchange of indices $j = 1, 2$; here I is the identity matrix. This is an expansion in the small parameter $\varepsilon = \sqrt{R_1 R_2}/l_0 \ll 1$. The fluid interaction term arises because the motions of the two particles are coupled through the fluid: motion of one particle gives a dipole flow field that then gives a force on the other particle. Note that we could include further terms in our expansions; however our philosophy is to obtain the simplest system that can usefully demonstrate unidirectional swimming at the lowest order in powers of ε. We expect that corrections for finite ε will not give major qualitative changes; plainly a full solution of the governing PDEs for Stokes flow would be needed for accurate results.

Applying the Lagrangian equations (2.10) gives the momenta

$$\boldsymbol{P} = (\nu_1+\nu_2)\dot{\boldsymbol{X}} + (\nu_1\chi_1 - \nu_2\chi_2)(\dot{s}\hat{\boldsymbol{r}} + s\dot{\phi}\hat{\boldsymbol{\phi}}), \tag{2.13}$$

$$p_s = (\nu_1\chi_1 + \nu_2\chi_2)\dot{s} + (\nu_1\chi_1 - \nu_2\chi_2)\hat{\boldsymbol{r}}\cdot\dot{\boldsymbol{X}}, \tag{2.14}$$

$$p_\phi = (\nu_1\chi_1 + \nu_2\chi_2)s^2\dot{\phi} + (\nu_1\chi_1 - \nu_2\chi_2)s\hat{\boldsymbol{\phi}}\cdot\dot{\boldsymbol{X}}. \tag{2.15}$$

The generalised forces are

$$\boldsymbol{Q} = -6\pi\eta(R_1+R_2)\dot{\boldsymbol{X}} + \frac{9\pi}{2}\frac{\eta R_1 R_2}{s}[2(\hat{\boldsymbol{r}}\hat{\boldsymbol{r}} + I)\cdot\dot{\boldsymbol{X}} + (\chi_1-\chi_2)(2\dot{s}\hat{\boldsymbol{r}} + s\dot{\phi}\hat{\boldsymbol{\phi}})] + \cdots, \tag{2.16}$$

$$Q_s = -6\pi\eta(\chi_1^2 R_1 + \chi_2^2 R_2)\dot{s} + \frac{9\pi}{2}\frac{\eta R_1 R_2}{s}[(\chi_1-\chi_2)2\hat{\boldsymbol{r}}\cdot\dot{\boldsymbol{X}} - 4\chi_1\chi_2\dot{s}] + \cdots, \tag{2.17}$$

$$Q_\phi = -6\pi\eta(\chi_1^2 R_1 + \chi_2^2 R_2)s^2\dot{\phi} + \frac{9\pi}{2}\frac{\eta R_1 R_2}{s}[(\chi_1-\chi_2)s\hat{\boldsymbol{\phi}}\cdot\dot{\boldsymbol{X}} - 2\chi_1\chi_2 s^2\dot{\phi}] + \cdots. \tag{2.18}$$

In each case the leading term is Stokes drag and the next term gives the effect of fluid interactions.

Now we consider what happens when only the leading order Stokes drag terms in (2.16–2.18) are retained. With these, and the kinetic and potential energies substituted into the Lagrangian prescription (2.10) we obtain the leading order equations first for what we will refer to as the *internal dynamics* of the swimmer given by the functions $(s(t), \phi(t))$

$$\begin{aligned}[\dot{p}_s - (\nu_1\chi_1+\nu_2\chi_2)s\dot{\phi}^2 - (\nu_1\chi_1-\nu_2\chi_2)\dot{\phi}\hat{\boldsymbol{\phi}}\cdot\dot{\boldsymbol{X}}] + 6\pi\eta(\chi_1^2R_1+\chi_2^2R_2)\dot{s} + k(s-l_0)&\\ = \frac{3\mu_0 m_1 m_2}{4\pi s^4}[\cos(\alpha_2-\alpha_1) - 3\cos\alpha_1\cos\alpha_2],&\end{aligned} \tag{2.19}$$

$$\dot{p}_\phi + 6\pi\eta(\chi_1^2R_1+\chi_2^2R_2)s^2\dot{\phi} = -B_{\text{ext}}b[m_1\sin(\phi+\alpha_1-\psi) + m_2\sin(\phi+\alpha_2-\psi)]. \tag{2.20}$$

We also have the equation for the evolution of the centre of reaction $\boldsymbol{X}$,

$$\dot{\boldsymbol{P}} = -6\pi\eta(R_1+R_2)\dot{\boldsymbol{X}}. \tag{2.21}$$

We integrate this equation and note that $\boldsymbol{P}$ must be bounded during the motion as must P_s, P_ϕ and s (but *a priori* ϕ or $\boldsymbol{X}$ need not be, to allow tumbling motion or unidirectional swimming). However from the integrated equation we see that $\boldsymbol{X}$ is in fact bounded in time, and so no unidirectional swimming is possible at this level of

approximation, with or without inertia. As argued in [24], to obtain unidirectional motion we need to include the leading fluid interaction term in (2.16), to yield

$$\dot{\boldsymbol{P}} = -6\pi\eta(R_1+R_2)\dot{\boldsymbol{X}} + \frac{9\pi}{2}\,\frac{\eta R_1 R_2}{s}\,[2(\hat{\boldsymbol{r}}\hat{\boldsymbol{r}}+I)\cdot\dot{\boldsymbol{X}} + (\chi_1-\chi_2)(2\dot{s}\hat{\boldsymbol{r}} + s\dot{\phi}\hat{\boldsymbol{\phi}})]. \tag{2.22}$$

In our philosophy of making the simplest model of the swimmer, we include this fluid interaction term, giving the possibility of unidirectional swimming of $\boldsymbol{X}$ at a rate linked to the small parameter ε. However we do not include the fluid interaction terms in the equations (2.19,2.20) for s and ϕ, which would give unimportant corrections of order ε. In short, we retain only leading drag effects in the internal dynamics for $(s(t), \phi(t))$.

We now consider the evolution of the magnetic beads in the externally imposed magnetic field. We model the internal dynamics of the magnetic dipole directions $\alpha_j(t)$ as minimising a magnetic energy

$$E_j = -\boldsymbol{M}_j\cdot\boldsymbol{H}_{\rm ext} + K_j\sin^2\alpha_j, \tag{2.23}$$

for $j=1,2$. Here $\boldsymbol{B}_{\rm ext} = \mu_0\boldsymbol{H}_{\rm ext}$, $\boldsymbol{M}_jV_j = \boldsymbol{m}_j$ where V_j is the volume of each magnet, and K_j are uniaxial anisotropy constants. This minimisation occurs on a very fast, nanosecond time scale, much shorter than that associated with the motion of the beads or the time-dependence of the external magnetic field. For this reason the equations for α_j are decoupled from the Lagrangian description and the above energies are not included in L. It is also important to note that in our modelling this minimisation affects only the *directions* of the magnetic dipoles, not their magnitudes. In order to include these magnetic effects in our ODE system we set

$$\kappa_j = K_j/(K_j + M_jH_{\rm ext}), \tag{2.24}$$

and use a gradient flow on a nanosecond time scale τ to minimise the energy through

$$\tau\dot{\alpha_j} = (1-\kappa_j)b\sin(\psi-\phi-\alpha_j) - \kappa_j\sin 2\alpha_j. \tag{2.25}$$

Thus in our formulation the parameter $\kappa_j = 1$ (for each bead $j=1,2$) corresponds to a hard magnet (for $\tau=0$, $\alpha_j=0$ is fixed) and $\kappa_j=0$ is the soft case (for $\tau=0$, $\alpha_j=\psi-\phi$ and so follows the external field). For intermediate values of κ_j the direction of the magnetic dipole is intermediate between the minima of $\sin^2\alpha_j$, that is $\alpha_j=0$ or π, and the direction of the external field; for the dipole direction to switch its principal alignment from say $\alpha_j=0$ to $\alpha_j=\pi$ it is required that $\kappa_j\le 1/2$ (given that $b\le 1$). How often such switching occurs depends on the time-dependent geometry and variation of magnetic field magnitude b. For values of κ_j around 0–0.2, though, the soft magnet switches frequently, following the external field in our simulations.

Note that we have neglected the field of the other bead in (2.23), it could easily be included but is small in comparison with the external field; by contrast it is the large *gradients* of the bead fields that are significant in driving the s component of motion.

2.2 *Non-dimensionalisation*

The complete set of parameters governing the system is

$$\mathcal{P} = \{l_0, R_j, k, \eta, \nu_j, \omega, B_{\rm ext}, m_j, \kappa_j, \tau\}. \tag{2.26}$$

We use the following basic dimensional units,

$$l_0 = \mathcal{L}, \quad \omega^{-1} = \mathcal{T}, \quad k\omega^{-2} = \mathcal{M}, \tag{2.27}$$

and define the dimensionless quantities,

$$\varpi = \varepsilon \frac{\mathcal{L}\mathcal{T}}{\mathcal{M}} 6\pi\eta(\chi_1^2\rho + \chi_2^2\rho^{-1}), \quad \upsilon = \frac{\sqrt{\nu_1\nu_2}}{\varpi^2\mathcal{M}}, \tag{2.28}$$

$$A_{\mathrm{mag}} = \frac{3\mu_0 m_1 m_2}{4\pi}\frac{\mathcal{T}^2}{\mathcal{M}\mathcal{L}^5}, \quad A_{\mathrm{ext}} = \sqrt{m_1 m_2}\, B_{\mathrm{ext}}\frac{\mathcal{T}^2}{\mathcal{M}\mathcal{L}^2}, \quad \varsigma = \frac{\tau}{\varpi\mathcal{T}}, \tag{2.29}$$

$$\rho = \sqrt{\frac{R_1}{R_2}}, \quad \mu = \sqrt{\frac{\nu_1}{\nu_2}}, \quad \sigma = \sqrt{\frac{m_1}{m_2}}, \quad \varepsilon = \frac{\sqrt{R_1 R_2}}{\mathcal{L}}. \tag{2.30}$$

We begin by neglecting inertia effects in a Stokes regime: this is based on the smallness of the parameter υ in our applications (see table 1 below). From now on we place a star on the dimensional variables used so far, and use unstarred quantities for the dimensionless variables, with

$$s^* = \mathcal{L}s, \quad t^* = \mathcal{T}t, \quad \boldsymbol{X}^* = \mathcal{L}\boldsymbol{X}. \tag{2.31}$$

The dimensionless governing equations are

$$\varpi\dot{s} + s - 1 = A_{\mathrm{mag}} s^{-4}\left[\cos(\alpha_2 - \alpha_1) - 3\cos\alpha_1\cos\alpha_2\right], \tag{2.32}$$

$$\varpi s^2\dot{\phi} = A_{\mathrm{ext}} b[\sigma\sin(\psi - \phi - \alpha_1) + \sigma^{-1}\sin(\psi - \phi - \alpha_2)], \tag{2.33}$$

together with equations for the directions of the magnetic dipoles,

$$\varsigma\varpi\dot{\alpha}_j = (1 - \kappa_j)b\sin(\psi - \phi - \alpha_j) - \kappa_j\sin 2\alpha_j. \tag{2.34}$$

We also have the equation for the motion of the centre of reaction from (2.22) (dropping $\dot{\boldsymbol{P}}$ from the neglect of inertia and the second $\dot{\boldsymbol{X}}$ term by virtue of $\varepsilon \ll 1$),

$$(\rho + \rho^{-1})\boldsymbol{X} = -\frac{3\varepsilon}{4}(\chi_2 - \chi_1)\int_0^t s^{-1}(2\dot{s}\hat{\boldsymbol{r}} + s\dot{\phi}\hat{\boldsymbol{\phi}})\, dt. \tag{2.35}$$

These equations contain the dimensionless parameters defined above,

$$\mathcal{P} = \{\varpi, A_{\mathrm{mag}}, A_{\mathrm{ext}}, \varsigma, \rho, \mu, \sigma, \varepsilon, \kappa_j\}, \tag{2.36}$$

and the input functions $\psi = \psi(t)$ and $b = b(t)$ are now 2π-periodic. The first two equations for the internal dynamics of the swimmer are now completely decoupled from $\boldsymbol{X}$. These can be time stepped and then the position $\boldsymbol{X}$ of the centre of reaction integrated.

We use the parameter set in table 1, appropriate for a typical, planned experimental realisation of a microscale swimmer, for example two magnets made of transition metals, attached to a red cell, vesicle, polymer or protein fibre whose elastic properties can be altered chemically. Some parameters, $\{\rho, \mu, \sigma\}$, are geometrical and take values of order unity, involving the ratios between dimensions of the particles and corresponding magnetic properties. There is not much interest in varying these here. The parameter ε is assumed to be small but in fact only enters as a multiplicative factor in any unidirectional swimming of the centre of reaction $\boldsymbol{X}$. Although we have neglected inertial terms by arguing that υ is small in applications, we retain possible magnetic hysteresis or switching effects and so keep the terms involving ς.

$l_0 = 4R_1 = 8R_2$	6.4×10^{-6}	m	ϖ	0.0503
k	0.05	N/m	υ	2.64×10^{-3}
η	0.1	Pa s	A_{mag}	0.0403
$\nu_1 = 8\nu_2$	1.51×10^{-13}	kg	A_{ext}	0.207
ω	2500	rad/s	ς	4.97×10^{-5}
B_{ext}	0.05	T	ρ	$\sqrt{2}$
$m_1 = 8m_2$	2.40×10^{-11}	A m^2	μ	$2\sqrt{2}$
τ	10^{-9}	s	σ	$2\sqrt{2}$
$\mathcal{L}$	6.4×10^{-6}	m	ε	$2^{-5/2}$
$\mathcal{T}$	4×10^{-4}	s	κ_1	0
$\mathcal{M}$	8×10^{-9}	kg	κ_2	0.5
			A	1.45
			(α, β)	$(1, 0.02)$

Table 1 Dimensional (left) and dimensionless (right) parameters for our simulations.

We consider the external field $\boldsymbol{b}(t)$ given by

$$b_x \equiv b\cos\psi = \alpha\cos t, \quad b_y \equiv b\sin\psi = \beta\sin t, \tag{2.37}$$

in dimensionless variables with α, β non-zero to avoid degenerate cases. Although our non-dimensionalisation implies the value $\alpha = 1$, we leave α arbitrary as it gives more mathematical structure to the formulae derived below. Considering the full equation set (2.34, 2.32–2.37), we note two symmetries

$$\{t, \phi, \psi, \boldsymbol{X}, \boldsymbol{b}\} \to \{t + \pi, \phi + \pi, \psi + \pi, -\boldsymbol{X}, -\boldsymbol{b}\}, \tag{2.38}$$

$$\{\phi, \psi, \alpha_j, X_2, b_2, \beta\} \to \{-\phi, -\psi, -\alpha_j, -X_2, -b_2, -\beta\} \tag{2.39}$$

(holding all other quantities and variables fixed). The first of these is a π rotation: if turned through an angle π, the swimmer can equally well swim in the $-\boldsymbol{X}$ direction. The second symmetry is a reflection in the y-axis and concerns moving from a magnetic field that rotates anti-clockwise (as in this paper) with one rotating clockwise (as in [22]). We will therefore take $\alpha > \beta > 0$ in what follows (generally avoiding the special cases when equalities hold).

Also in figure 1 we placed the smaller particle as particle 2 on the left-hand side, and with this it follows that $\chi_1 < \chi_2$ as depicted. In fact we may as well always define particle 2 to be smaller than particle 1 so that $\hat{\boldsymbol{r}}$ goes from smaller to larger and the azimuthal direction $\hat{\boldsymbol{\phi}}$ is then defined via a $+\pi/2$ rotation. In short, to simplify discussion in what follows, we will adopt the conventions that

$$1 = \alpha > \beta > 0, \quad \chi_2 > \chi_1. \tag{2.40}$$

(Note that if $\chi_1 = \chi_2$ then $\boldsymbol{X}$ in (2.35) is constant to any order by symmetry.) The equation (2.35) for the motion of the centre of reaction already gives us a little useful information. We can observe that the radial, $\hat{\boldsymbol{r}}$ component of $\dot{\boldsymbol{X}}$ is proportional to $-2s^{-1}\dot{s}$ and the angular $\hat{\boldsymbol{\phi}}$ component is proportional to $-\dot{\phi}$. Given that s does not vary much from unity in all our simulations, this is approximately $\dot{\boldsymbol{X}} \propto -2\dot{s}\hat{\boldsymbol{r}} - s\dot{\phi}\hat{\boldsymbol{\phi}}$ and so we obtain:

Rule of thumb 1: *the motion of the centre of reaction $\boldsymbol{X}$ is in phase with the motion of the smaller particle,*

and out of phase with that of the larger particle. The motion of $\boldsymbol{X}$ is similar to that of the smaller particle but, relatively, the radial component is exaggerated by a factor of two.

While the function $\boldsymbol{X}$ in (2.35) gives the actual path of the centre of reaction, in the mathematical development it is useful to integrate it by parts to obtain

$$(\rho+\rho^{-1})\boldsymbol{X} = (\rho+\rho^{-1})\boldsymbol{X}_{\rm int} - \frac{3\varepsilon}{4}(\chi_2-\chi_1)\big[2\log s\,\hat{\boldsymbol{r}}+\hat{\boldsymbol{r}}\big]_0^t, \tag{2.41}$$

with the new position $\boldsymbol{X}_{\rm int}$ given by the integral

$$(\rho+\rho^{-1})\boldsymbol{X}_{\rm int} = \frac{3\varepsilon}{4}(\chi_2-\chi_1)\int_0^t 2\log s\,\dot{\phi}\hat{\boldsymbol{\phi}}\,dt. \tag{2.42}$$

Here from the point of view of finding unidirectional swimming, the boundary terms in (2.41) may be discarded as they are bounded in time. Although they are important in giving the actual path $\boldsymbol{X}(t)$, for persistent unidirectional motion it is sufficient that $|\boldsymbol{X}_{\rm int}|\to\infty$ as $t\to\infty$.

Note finally that there is a natural limit on the magnitude of $A_{\rm mag}$ in the design of a swimmer: if it is too large the swimmer will collapse with $s\to 0$ following from the increasing s^{-4} dipole attraction. Collapse from $s=1$ becomes inevitable (for aligned dipoles) when the potential $g(s)=1-s-2A_{\rm mag}s^{-4}$ satisfies $g'(s)=g(s)=0$ for some s and this gives the limit

$$A_{\rm mag} < A_{\rm mag}^{\max} = 8^{-1}(5/4)^{-5} \simeq 0.04096. \tag{2.43}$$

3. Simulations and theory

3.1 *Simulations of the full system*

We will now consider the equation set (2.32–2.35), together with the specification of the external field (2.37). We refer to this as the 'full system' in which only inertia has been neglected. We start with the standard set of parameters used in table 1. In order to elucidate different regimes, we will vary as few parameters as posible from these values. Our aim is to present some examples of swimming before we start to simplify the problem. For convenience we set $T=2\pi$ and note that the simulations are started with $s(0)=1$, $\phi(0)=0$ and $\boldsymbol{X}(0)=0$, except in some later plots where the initial angle $\phi(0)$ is increased to avoid a long transient (for example in figure 6(g) below).

Figure 2 shows simulations of the full system with parameters as in table 1. Note that as $\kappa_1=0$, magnet 1 is entirely soft; given the small value of $\varsigma\varpi$ the equation for this magnet, (2.34) for $j=1$, gives $\alpha_1\simeq\psi-\phi$ to a good approximation. Panel 2(a) shows $s(t)$ rapidly settling to a periodic oscillation with values around unity. Panel (b) indicates that $\phi(t)$ shows fairly large oscillations about $\pi/2$ after a short transient. As the values of $\phi(t)$ are bounded we will refer to this as a 'trapping' regime: the angle ϕ does not increase (or decrease) secularly. Panel (c) is a useful diagnostic tool which is to plot the resulting limit cycle (taken late in the run) of the internal dynamics with $s(t)$ and $\phi(t)$ as polar coordinates. This shows a figure of eight loop traversed in the direction of the arrow (predominantly clockwise), and gives the leading order trajectories of the two beads relative to the centre of reaction.[†] The swinging motion seen in figure 2 (and in other figures below) resembles

[†] Note that our results differ in detail from those in [25], as this paper includes a non-central component to the force between the dipoles, which is not present in the Lagrangian formulation.

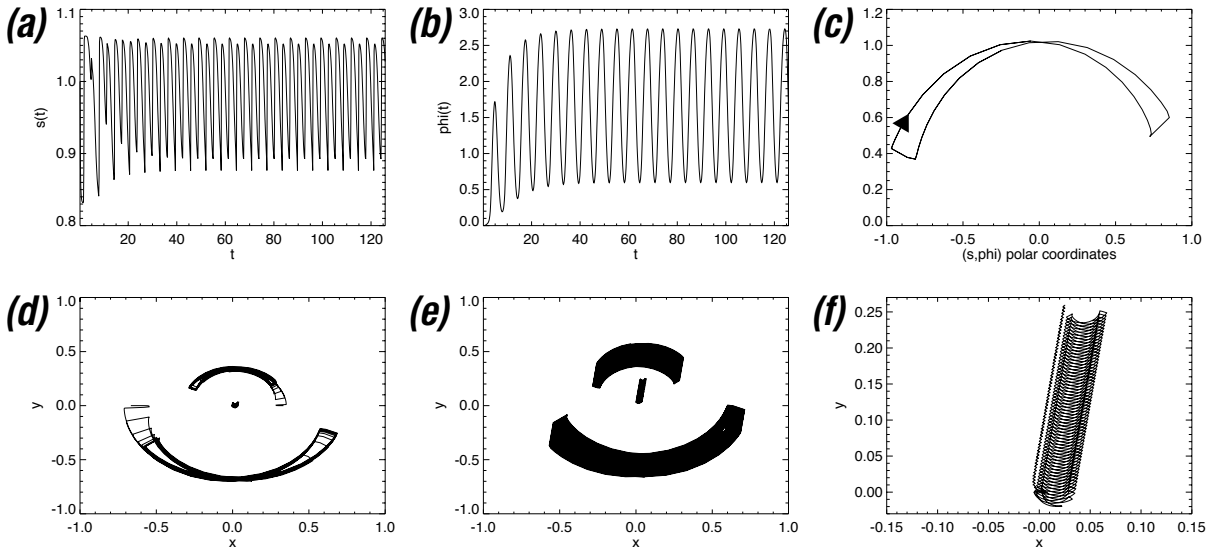

Fig. 2 Simulation of the full system with parameters as in table 1. Depicted are (a) $s(t)$ and (b) $\phi(t)$ for $0 \leq t \leq 20T$, (c) phase plane limit cycle in (s, ϕ) polar coordinates, (d) $\boldsymbol{r}_1(t)$, $\boldsymbol{r}_2(t)$ and $\boldsymbol{X}(t)$ in the (x, y) plane for $0 \leq t \leq 10T$, (e) $\boldsymbol{r}_1(t)$, $\boldsymbol{r}_2(t)$ and $\boldsymbol{X}(t)$ in the (x, y) plane for $10T \leq t \leq 60T$ (f) $\boldsymbol{X}(t)$ and $\boldsymbol{X}_{\rm int}(t)$ in the (x, y) plane for $0 \leq t \leq 60T$.

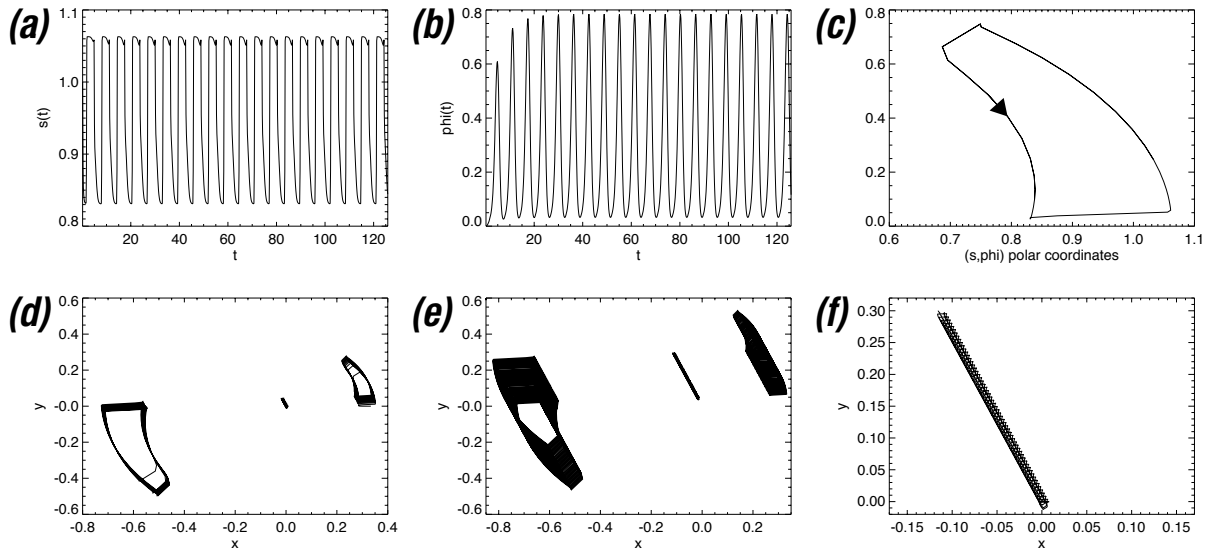

Fig. 3 Simulation as in figure 2 with parameters from table 1, except for $\kappa_2 = 1$ giving the soft–hard system.

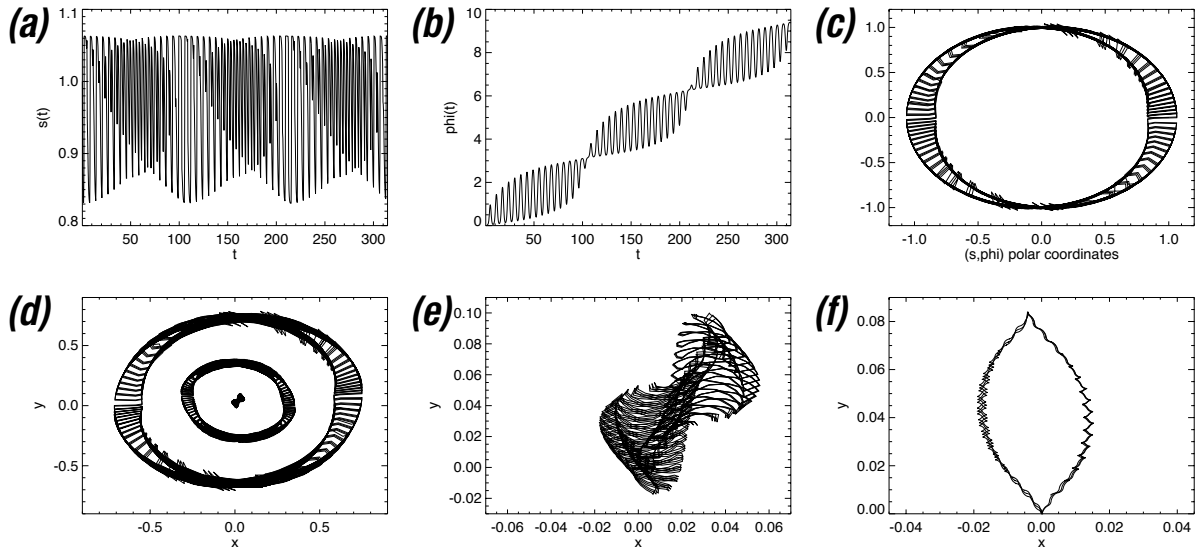

Fig. 4 Simulation of the full system with parameters from table 1, except for $\kappa_2 = 0.7$. Depicted are (a) $s(t)$ and (b) $\phi(t)$ for $0 \leq t \leq 50T$, and (c) phase plane with (s, ϕ) polar coordinates, (d) $\boldsymbol{r}_1(t)$, $\boldsymbol{r}_2(t)$ and $\boldsymbol{X}(t)$ in the (x, y) plane, (e) $\boldsymbol{X}(t)$ and (f) $\boldsymbol{X}_{\rm int}(t)$ in the (x, y) plane, for $0 \leq t \leq 100T$.

closely that considered in the general discussion of two-bead swimmers in [14; 15; 16]. It is worth noting that in our system the external magnetic field exerts a net torque on the swimmer (and so on the fluid) which need not necessarily have a zero time-average: as such our swimmer falls into the class considered in [15], whereas those with identically zero torque are discussed in [16].

Whilst panels 2(a,b,c) involve only the internal dynamics, panels (d,e) reconstruct the swinging motion of the swimmer for short and long times respectively. For simplicity let us refer to the $+x$ direction as East (E), the $+y$ direction as North (N), etc., defined relative to the elliptical polarisation of the external field. Given this, the larger bead is to the N and undergoes a smaller amplitude motion than the small bead to the S. In the centre is plotted the centre of reaction $\boldsymbol{X}$. The fluid interactions then give a motion of the whole swimmer northwards, or more accurately NNE. Panel (f) shows the motion of the centre of reaction in more detail. There are two curves plotted here: the right-hand one is $\boldsymbol{X}$: aside from the drift, the motion follows rule of thumb 1. The curve close and to its left is $\boldsymbol{X}_{\rm int}$. Figure 2 shows clear evidence of unidirectional motion, and longer runs show no departure from the regime depicted.

Having established this, it is now of interest to turn off and on various effects and explore something of parameter space: we have observed that one key aspect is the role of the soft/hard magnets. To see this, figure 3 shows a run of the full system with the parameter values in table 1, except for setting $\kappa_2 = 1$. Thus magnet 1 is entirely soft and magnet 2 entirely hard: we call this the 'soft–hard system'. Here provided $\varsigma\varpi$ is small enough (as it is in table 1) we have, to a very good approximation,

$$\alpha_1 = \psi - \phi, \quad \alpha_2 = 0. \tag{3.1}$$

We now observe somewhat different behaviour from that in figure 2: in panel (c) we see anticlockwise motion

in a simple loop for the internal dynamics limit cycle with ϕ a little larger than zero. Panels (b,d,e) confirm that the swimmer rocks about a mean angle around 0.4 radians (20°). With this is motion of the centre of reaction in a NW direction, panel (f); in this panel the trace of $\boldsymbol{X}$ is visible, but obscures that for $\boldsymbol{X}_{\rm int}$ which shows smaller oscillations.

Figure 2 for $\kappa_2 = 0.5$ and figure 3 for $\kappa_2 = 1$ have many differences, which suggests investigating intermediate values. Figure 4 shows the case $\kappa = 0.7$. Panels (a,b,c) again show the internal dynamics of the system, and we now see that the angle ϕ drifts secularly, in panel (b) and in the phase space panel (c). We refer to this as a non-trapping regime. The motions of the beads and the centre of reaction are shown in panel (d). At various times the motion is similar to that in the trapped case (figure 3) but the persistent increase in ϕ means that after a time the swimmer has rotated by π and any significant translation of the swimmer is then carefully undone. This is clear in the traces in panels (e,f) of $\boldsymbol{X}$ and of $\boldsymbol{X}_{\rm int}$, which shows a particularly simple form.

Figures 2–4 encapsulate what we need to understand. In the first two figures the trapping of the angle ϕ is crucial to ensuring unidirectional motion. In view of the symmetry (2.38), if ϕ is allowed to increase through π the motion is likely to then be reversed.† In short, trapping of the angle ϕ is vital, but by what mechanisms can this occur and which parameters are important? What distinguishes the persistent motions in figures 2 and 3 and why does the intermediate case in figure 4, perhaps suprisingly, simply show slow motion in a closed path? Can we extract any more useful rules of thumb about the directions or types of motion that can occur?

3.2 *Model* 0*: simplest model*

In our analytical investigations our aim now is to simplify the problem as much as possible and then add effects one by one. We focus on the soft–hard system given by (2.32–2.37) with (3.1) and assume that

$$\varpi \ll 1, \quad A_{\rm mag} \ll 1. \tag{3.2}$$

With these we may drop the $\varpi\dot{s}$ term in (2.32) and with $s \simeq 1$ approximate $s^2 \simeq s^{-4} \simeq 1$ in (2.32,2.33), to leave the equations governing the internal dynamics as

$$s = 1 - 2A_{\rm mag}\cos(\psi - \phi), \quad \varpi\dot{\phi} = A_{\rm ext} b\sigma^{-1}\sin(\psi - \phi). \tag{3.3}$$

Together with this we approximate $\log s \simeq s - 1$ so that (2.42) becomes

$$(\rho + \rho^{-1})\boldsymbol{X}_{\rm int} = \frac{3\varepsilon}{4}(\chi_2 - \chi_1)\int_0^t 2(s-1)\dot{\phi}\hat{\boldsymbol{\phi}}\,dt. \tag{3.4}$$

We will retain the approximation $\varpi \ll 1$ in all of what follows: this balances the dipole attraction or repulsion against the spring force and throws away the viscous drag effect in the s equation. Including the viscous drag here does not appear to introduce any important new effects. On the other hand the viscous drag has to be left in the ϕ equation. The above approximations involving $s \simeq 1$ are useful simplifications that are well borne out in simulations (for example panels (a) of the above figures) and indeed if s is allowed to become too small the swimmer will collapse.

† Orbits in the (s, ϕ) phase space could exist which explore the full range of ϕ but are not invariant under (2.38) plus a time translation. However we have not observed such orbits, which are unlikely to be robust enough to be practically useful; we discount these to simplify discussion.

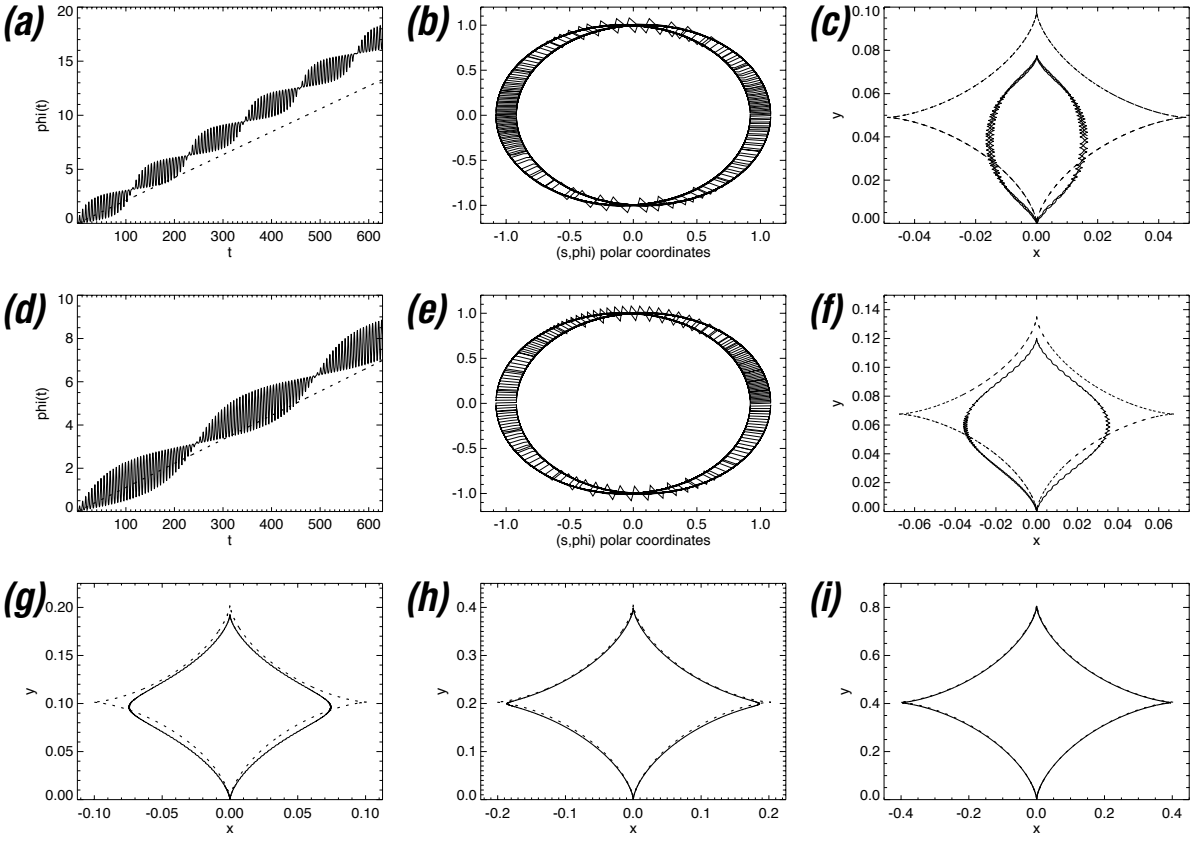

Fig. 5 Simulation of model 0. In (a,d) we show $\phi(t)$, (b,e) phase space with (s,ϕ) polar coordinates, and (c,f) $\boldsymbol{X}_{\rm int}$ in the (x,y) plane. In (a,b,c) parameters are as in table 1 but in (d,e,f) $A_{\rm ext}$ is changed to 0.15; in both cases $0 \le t \le 100T$. We also show $\boldsymbol{X}_{\rm int}$ in the (x,y) plane for (g) $A_{\rm ext} = 0.1$, (h) 0.05 and (i) 0.025 and t between 0 and $200T$, $800T$ and $3200T$ respectively.

It is now convenient to absorb as many constants as possible and we set

$$(\rho + \rho^{-1})\boldsymbol{X}_{\rm int} = (3\varepsilon/4)\,(\chi_2 - \chi_1)A_{\rm mag}\tilde{\boldsymbol{X}}_{\rm int}, \quad A = A_{\rm ext}/\varpi\sigma. \tag{3.5}$$

This gives a scaled centre of reaction $\tilde{\boldsymbol{X}}_{\rm int}$ and the governing equations are

$$\dot{\phi} = Ab\sin(\psi - \phi), \quad \tilde{\boldsymbol{X}}_{\rm int} = -\int_0^t 4\cos(\psi - \phi)\dot{\phi}\hat{\boldsymbol{\phi}}\,dt, \tag{3.6}$$

involving just a single parameter A, while s is a diagnostic given in (3.3).

We now integrate these equations and figure 5 shows the results (solid lines only). For comparison with earlier figures we reconstruct s from (3.3) and show $\boldsymbol{X}_{\rm int}$ in our plots, rescaled from $\tilde{\boldsymbol{X}}_{\rm int}$ via (3.5) using parameter values in table 1. Panels 5(a,b,c) show results for A with the value as in table 1. We are clearly not in a

trapping regime, as the angle $\phi(t)$ (panel (a)) shows a secular increase and the orbit in the (s,ϕ) phase space (panel (b)) encircles the origin symmetrically. For the motion of the centre of reaction, panel (c) shows $\boldsymbol{X}_{\rm int}$ (solid) which moves in a closed curve: there is no unidirectional motion. Reducing the value of A to 0.15 gives corresponding panels (d,e,f) and panels (g,h,i) give the motion of $\boldsymbol{X}_{\rm int}$ for other, smaller values; the path takes a star-like form with cusps. There appears to be no threshold for trapping of ϕ and unidirectional swimming: as A is reduced the swimmer spends a longer and longer time $t = O(A^{-2})$ describing a path of scale $O(A^{-1})$. Although model 0 is in a sense a failure, it is a useful starting point, and in fact the results in figure 5(a,b,c) are strikingly similar to those in the intermediate case of the full model in figure 4: compare the evolution of $\boldsymbol{X}_{\rm int}$ in figures 4(f) and 5(c) for shape and scale.

Model 0 can be studied asymptotically and is the basis of the approximation of more complex models. Within this model the only important differential equation is in (3.6) for ϕ, which can also be written as

$$\dot{\phi} = A(b_y\cos\phi - b_x\sin\phi) = A(\beta\sin t\cos\phi - \alpha\cos t\sin\phi) \tag{3.7}$$

from (2.37). Although not analytically soluble, it is amenable to asymptotic methods. We consider the limit of small A and pose the expansion,

$$\phi = \phi_0 + A\phi_1 + A^2\phi_2 + \cdots, \tag{3.8}$$

where the ϕ_i are functions of time t and a long time scale $\tau = A^2 t$, which will be used to remove secular terms. We substitute in (3.7) which yields

$$\begin{aligned}(\partial_t + A^2\partial_\tau)(\phi_0+\phi_1+\cdots) = {}& Ab_y[\cos\phi_0 - (A\phi_1+\cdots)\sin\phi_0 - \cdots] \\ & -Ab_x[\sin\phi_0 + (A\phi_1+\cdots)\cos\phi_0 - \cdots].\end{aligned} \tag{3.9}$$

At leading order $\partial_t\phi_0 = 0$ and so we may set $\phi_0 = \overline{\phi}_0(\tau)$, varying only on the long time scale. Then we have for ϕ_1,

$$\partial_t\phi_1 = b_y\cos\overline{\phi}_0 - b_x\sin\overline{\phi}_0. \tag{3.10}$$

With b_x and b_y defined in (2.37), we then obtain

$$\phi_1 = \overline{\phi}_1(\tau) - \beta\cos t\cos\overline{\phi}_0 - \alpha\sin t\sin\overline{\phi}_0. \tag{3.11}$$

At order A^2 equation (3.9) has secular terms, and taking the average $\langle\cdot\rangle$ over the fast t time scale yields the equation for ϕ_0 in the long τ time scale as

$$\partial_\tau\overline{\phi}_0 = -\langle b_y\phi_1\rangle\sin\overline{\phi}_0 - \langle b_x\phi_1\rangle\cos\overline{\phi}_0 = \alpha\beta/2. \tag{3.12}$$

This integrates to give

$$\phi_0 = \overline{\phi}_0 = \alpha\beta\tau/2 \equiv \Omega_0 t, \quad \Omega_0 \equiv \tfrac{1}{2}\alpha\beta A^2 \tag{3.13}$$

and so the mean orientation $\overline{\phi}_0$ of the swimmer rotates slowly but persistently for small A. A further level of the expansion gives an equation for $\overline{\phi}_1(\tau)$ but because this involves cubic products of sines and cosines, there are no resonances and we may take $\overline{\phi}_1(\tau) = 0$.

We can now integrate $\boldsymbol{X}_{\rm int}$ in (3.6): we may average over the oscillations inside the integral (to do otherwise gives only a small correction). We note that at leading order

$$2A_{\rm mag}^{-1}\langle(s-1)\dot{\phi}\rangle = -4A\langle\cos(\psi-\overline{\phi}_0)\partial_t\phi_1\rangle = -4A\langle b^{-1}(b_x\cos\overline{\phi}_0 + b_y\sin\overline{\phi}_0)\partial_t\phi_1\rangle = 2A\Lambda\sin 2\overline{\phi}_0, \tag{3.14}$$

with

$$\Lambda(\alpha,\beta) = \left\langle (\alpha^2\cos^2 t - \beta^2\sin^2 t)(\alpha^2\cos^2 t + \beta^2\sin^2 t)^{-1/2} \right\rangle \tag{3.15}$$
$$= \frac{2}{\pi\alpha}\,\frac{\alpha^2}{\alpha^2-\beta^2}\left[(\alpha^2+\beta^2)\,\mathrm{E}(1-\alpha^2/\beta^2) - 2\beta^2\,\mathrm{K}(1-\beta^2/\alpha^2)\right].$$

written in terms of complete elliptic integrals; see section 17.3 of [27]. We note that

$$\Lambda \sim 2\alpha/\pi \quad (\beta/\alpha \to 0), \qquad \Lambda \sim \tfrac{3}{8}\alpha(1-\beta^2/\alpha^2) \quad (\beta/\alpha \to 1). \tag{3.16}$$

This leaves

$$\tilde{\boldsymbol{X}}_{\rm int} = \int_0^t 2A\Lambda \sin 2\overline{\phi}_0(-\sin\overline{\phi}_0, \cos\overline{\phi}_0)\,dt \tag{3.17}$$

which together with (3.13) integrates to yield the path as

$$\tilde{\boldsymbol{X}}_{\rm int} = \frac{4A\Lambda}{3\Omega_0}\,(-\sin^3\Omega_0 t, 1-\cos^3\Omega_0 t). \tag{3.18}$$

This completes our analysis of model 0 and approximate results for $\overline{\phi}_0$ and $\boldsymbol{X}_{\rm int}$ are shown dotted in figure 5. We see good qualitative agreement for the mean drift in ϕ in panels (a,d) and fair agreement for the motion of the swimmer via $\boldsymbol{X}_{\rm int}$ in panels (c,f). Note that the values of A are not particularly small here: panels (a,b,c) have $A_{\rm ext} = 0.207$ and $A = 1.45$ (table 1) so the agreement is very satisfactory. As A is further reduced the agreement improves for ϕ (not shown) and for the star-like path as shown in panels (g,h,i).

Note that in the integral (3.4) an important quantity is $\langle(s-1)\dot{\phi}\rangle$: at the leading order in our expansion this has to be non-zero for motion of the centre of reaction to occur. Suppose for a moment we ignore the slow drift in ϕ and suppose it is oscillating about some mean value. If at this time this quantity is positive the swimmer swims in the $+\hat{\boldsymbol{\phi}}$ direction (bearing in mind (2.40)). If we consider 'simple' motion of each particle, for example that depicted in figure 3(c), and correlate changes in $s-1$ to those of $\dot{\phi}$ we obtain the following.

Rule of thumb 2: *if the paths of each particle have an anti-clockwise sense, then the swimmer will move in the $+\hat{\boldsymbol{\phi}}$ direction, and if they have a clockwise sense then in the $-\hat{\boldsymbol{\phi}}$ direction. Furthermore, in a trapped regime the swimmer moves in the $\hat{\boldsymbol{\phi}}$ direction at a velocity roughly proportional to the signed area swept out in the (s,ϕ) phase space.*

This latter observation arises since with $s \simeq 1$, the signed area described by a limit cycle in the phase space with (s,ϕ) as polar coordinates is

$$\oint \tfrac{1}{2}s^2\,d\phi \simeq \int (s-1)\dot{\phi}\,dt = 2\pi\langle(s-1)\dot{\phi}\rangle, \tag{3.19}$$

and is a measure of the lack of time-reversibility of the internal dynamics [cf. 16]. We can also note for model 0 that $\langle(s-1)\dot{\phi}\rangle$ is given in equation (3.14) and is positive in the first and third quadrants of $\overline{\phi}_0$ and negative in the other two quadrants, bearing in mind (2.40). We then have the following.

Rule of thumb 3: *the particles show anti-clockwise motion if $\overline{\phi}_0$ lies in the first and third quadrants and clockwise motion otherwise: the direction of motion is then given by rule of thumb 2.*

We should make a few comments: we derived these rules from model 0 by taking out the slow drift in ϕ and using our small-A expansion. In the case of model 0 the rules work well for moderate periods of the motion, when the average angle ϕ is approximately constant. Over longer periods the average orientation of the swimmer slowly rotates, and the swimmer maps out the curve given in (3.18) and figure 5(c,d,g-i). For the initial part of the motion though, the swimmer first has $\overline{\phi}_0 = 0$ and swims NW. But then $\overline{\phi}_0$ slowly increases to $\pi/2$ and the swimmer stops at a cusp, the motion then reverses and it moves NE. As $\overline{\phi}_0$ further increases the motion becomes SE and SW. For each stage of the path the above rules apply. Figure 3, with ϕ trapped, fits the above rules of thumb while the picture is rather less clear for figure 2 since the limit cycle in panel (c) has a figure of eight shape, and the motion does not appear to be in the $\hat{\boldsymbol{\phi}}$ direction. In conclusion, model 0 does not give unidirectional motion as we have seen, and we can give the following.

Rule of thumb 4: *it is necessary and sufficient to trap the angle ϕ, that is to avoid unbounded secular increase or decrease, to obtain unidirectional motion of the centre of reaction.*

This then throws attention on the general equation (2.33) for ϕ: in writing down model 0 we have removed the s^2 term and made the two magnets completely hard and completely soft via (3.1). Clearly it makes sense to add these three effects individually to model 0 and see what kinds of trapping behaviour are present and what asymptotic approximations reveal. This gives us three models which we label as 0+*MoR*, 0+*nH* and 0+*nS*, and describe in more detail below.

3.3 *Model 0+MoR: trapping for varying moment of reaction*

Our first mechanism for trapping of the angle ϕ is to reintroduce the variation of viscous drag with the distance s between the two swimmers. To be specific, note that we have a familiar moment of inertia term, say $I_0 = (\nu_1\chi_1 + \nu_2\chi_2)s^2$ in (2.15) which varies with s and controls the rate at which angular momentum $I_0\dot{\phi}$ is imparted by a given external torque. In a Stokes regime this is absent but we have a closely analogous 'moment of resistance'† term $I_1 = 6\pi\eta(\chi_1^2 R_1 + \chi_2^2 R_2)s^2$ in (2.20), which controls the angular velocity driven by a given external torque. Including the variation of this quantity with s amounts to reinstating the s^2 term on the left-hand side of (2.33), to yield the following system which we refer to as model 0+*MoR*, rescaled as we did in (3.5),

$$s = 1 - 2A_{\mathrm{mag}}\cos(\psi - \phi), \quad \dot{\phi} = As^{-2}b\sin(\psi - \phi), \tag{3.20}$$

$$\tilde{\boldsymbol{X}}_{\mathrm{int}} = -\int_0^t 4\cos(\psi - \phi)\,\dot{\phi}\hat{\boldsymbol{\phi}}\,dt. \tag{3.21}$$

Note that although we have modified the ϕ equation we do not reintroduce s-dependent terms in other equations as these will not have qualitatively important effects. We are only pursuing the issue of trapping, and then unidirectional motion will follow.

We have now a second parameter A_{mag}, which is always numerically small, by virtue of (2.43). We therefore introduce it into the multiple scales analysis, as a parameter of order A. We must now multiply the right-hand side of (3.9) by

$$s^{-2} = 1 + 4A_{\mathrm{mag}}\cos(\psi - \overline{\phi}_0) + \cdots. \tag{3.22}$$

† Note that this is a component of the rotation tensor discussed in section 5.3 of [23] and termed there a principal moment of resistance.

The analysis from (3.8) onwards then goes through up to order A^2: when we eliminate secular terms at this order we obtain an additional contribution

$$A^2\partial_\tau\overline{\phi}_0 = \Omega_0 + 4AA_{\rm mag}\langle b^{-1}(b_x\cos\overline{\phi}_0 + b_y\sin\overline{\phi}_0)\partial_t\phi_1\rangle = \Omega_0 - 2AA_{\rm mag}\Lambda\sin 2\overline{\phi}_0, \tag{3.23}$$

where Λ is defined in (3.15). Restoring the t time scale we obtain for the mean orientation of the swimmer,

$$\frac{d\overline{\phi}_0}{dt} = \tfrac{1}{2}\alpha\beta A^2 - 2AA_{\rm mag}\Lambda\sin 2\overline{\phi}_0. \tag{3.24}$$

This ODE for $\overline{\phi}_0$ can be solved exactly but solutions are not particularly illuminating. The important point is that this can have fixed points, corresponding to trapped $\overline{\phi}_0$, which are solutions of

$$\sin 2\overline{\phi}_0 = \frac{\alpha\beta A}{4\Lambda A_{\rm mag}}\,, \tag{3.25}$$

provided the right-hand side is smaller than one (all parameters here have positive values). Thus the condition that the right-hand side of (3.25) is unity gives a threshold for trapping of the angle $\overline{\phi}_0$; above the threshold we are back in the regime of model 0, with indefinite increase of $\overline{\phi}_0$ and no unidirectional motion. When trapping occurs, there are four possible solutions in the range $-\pi < \overline{\phi}_0 \le \pi$, of which two are stable. It may be checked that one stable solution is given by taking the principal branch of the inverse sine function and so has $0 \le \overline{\phi}_0 \le \pi/4$, say E–NE, the other differs by π, say W–SW. We then have

$$\tilde{\boldsymbol{X}}_{\rm int} \simeq (-\sin\overline{\phi}_0, \cos\overline{\phi}_0)\tilde{V}t, \quad \tilde{V} = 2A\Lambda\sin 2\overline{\phi}_0 = \alpha\beta A^2/2A_{\rm mag} \tag{3.26}$$

as $t\to\infty$, so it moves with speed $\tilde{V}$ in a direction of $\overline{\phi}_0 + \pi/2$, namely N–NW or S–SE.

Figure 6 shows simulations of equations (3.20–3.21) of model 0+*MoR* for three parameter sets: solid lines give numerical results and dotted lines theory from (3.8), (3.11), (3.20), (3.25) and (3.26), which improves as we go down the rows of panels. All three simulations show ϕ trapping in panels (a,d,g) and convergence to a limit cycle in panels (b,e,h) with anti-clockise motion. Together with this we have motion to NNW in panels (c,f,i) in a direction in good agreement with both rules 2 and 3 and with the asymptotic theory. We can also make a useful comparison of the results in panels 6(a,b,c) with 3(c,f), the soft–hard system: the behaviour in phase space and the direction of motion are very similar. We can thus identify the dominant trapping mechanism in the soft–hard system of figure 3 as the variation of the moment of resistance with s as isolated in model 0+*MoR*. We can distil our intuition into the following.

Rule of thumb 5: *when the dominant mechanism for ϕ trapping is from the variation of the moment of resistance and unidirectional swimming occurs, the average swimmer orientation is in the direction E–NE or W–SW and motion is in the direction N–NW or S–SE.*

3.4 *Model 0+nH: trapping for a nearly hard magnet*

Having found a trapping mechanism in model 0+*MoR* through the introduction of the s^2 term in the ϕ equation, we now return to model 0 and include a magnetic effect instead. In model 0+*nH* we replace the hard magnet 2 by a general magnet. Thus we specifiy a value of κ_2 and evolve the magnetic dipole angle α_2 by means of equation (2.34) with $j = 2$. We may also use perturbation theory to study the case $\kappa_2 \simeq 1$ when the magnet is

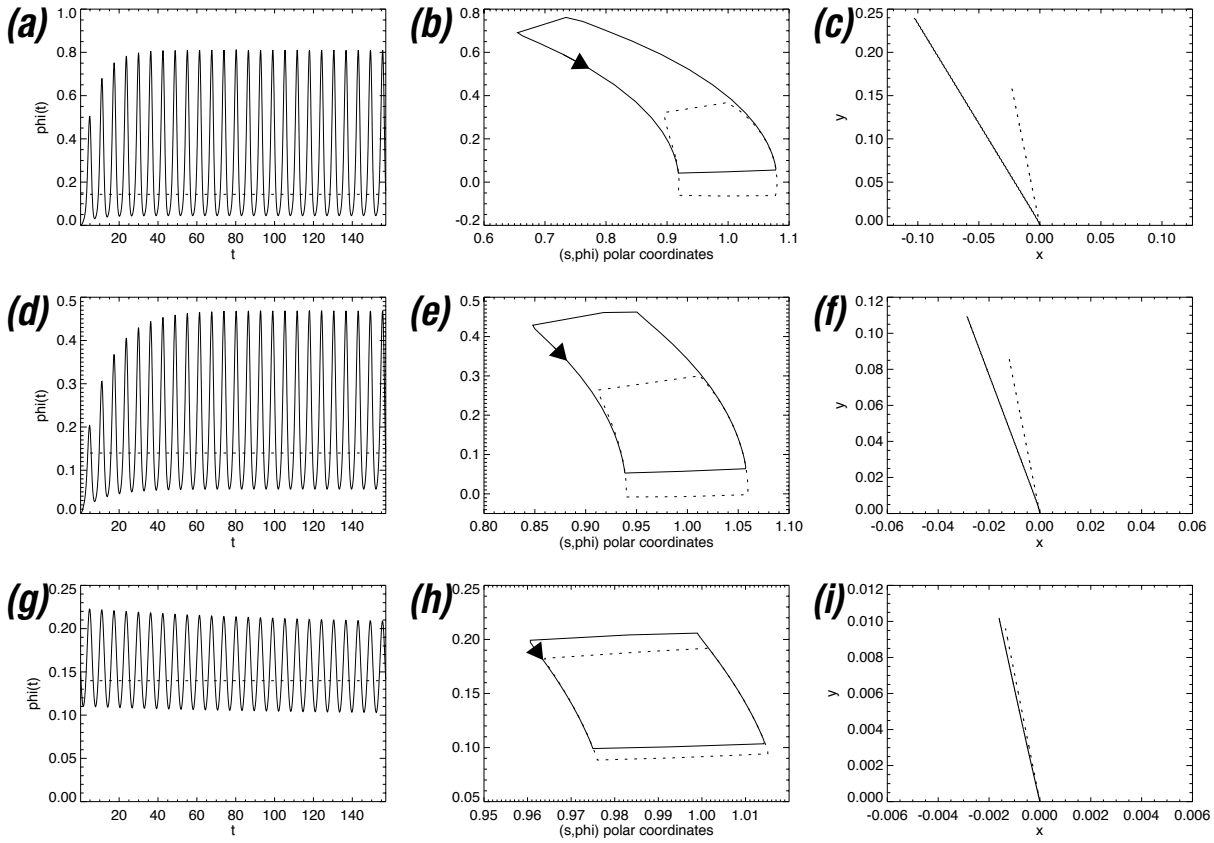

Fig. 6 Simulation of model 0+*MoR*. In (a,d,g) we show $\phi(t)$ for $0 \le t \le 25T$, (b,e,h) limit cycle in phase space with (s,ϕ) polar coordinates, and (c,f,i) $\boldsymbol{X}_{\rm int}$ in the (x,y) plane for $0 \le t \le 60T$. In (a,b,c) parameters are as in table 1 but in (d,e,f) $A_{\rm ext} = 0.15$, $A_{\rm mag} = 0.03$, and in (g,h,i) $A_{\rm ext} = 0.05$ and $A_{\rm mag} = 0.01$.

'nearly hard' hence the name 0+nH for this model where the nH stands for not hard or for nearly hard. We keep the other bead as a completely soft magnet with $\alpha_1 = \psi - \phi$ and set $s \simeq 1$ at leading order, excluding the s^2 term that we retained in the ϕ-equation of model 0+*MoR*; this is both to isolate the effect and because in our asymptotic theory the effects may be added together in any case. The relevant (rescaled) equations are

$$s = 1 - 2A_{\rm mag}[\cos(\psi-\phi)\cos\alpha_2 - \tfrac{1}{2}\sin(\psi-\phi)\sin\alpha_2], \tag{3.27}$$

$$\dot{\phi} = Ab\sin(\psi-\phi-\alpha_2), \tag{3.28}$$

$$\varsigma\varpi\dot{\alpha}_2 = (1-\kappa_2)b\sin(\psi-\phi-\alpha_2) - \kappa_2\sin 2\alpha_2, \tag{3.29}$$

$$\tilde{\boldsymbol{X}}_{\rm int} = -\int_0^t 4[\cos(\psi-\phi)\cos\alpha_2 - \tfrac{1}{2}\sin(\psi-\phi)\sin\alpha_2]\dot{\phi}\hat{\boldsymbol{\phi}}\,dt. \tag{3.30}$$

This system is parameterised now by A, κ_2 and $\varsigma\varpi$. Mathematically we can take a limit in which the magnet

is nearly hard with $\alpha_2 \ll 1$ and $1-\kappa_2 \ll 1$. Taking also $\varsigma\varpi = 0$, this yields for the small change in the hard dipole angle, at leading order,

$$\alpha_2 = \tfrac{1}{2}(1-\kappa_2)b\sin(\psi - \overline{\phi}_0). \tag{3.31}$$

This can now be fed into the multiple scales expansion. From (3.28), we need to introduce a term $-A\alpha_2 b\cos(\psi - \overline{\phi}_0)$ to the right-hand side of (3.9). Taking $1-\kappa_2 = O(A)$ and averaging, the equation for the slow evolution of $\overline{\phi}_0$ becomes

$$A^2\partial_\tau\overline{\phi}_0 = \Omega_0 - A\langle\alpha_2 b\cos(\psi-\overline{\phi}_0)\rangle = \Omega_0 + \tfrac{1}{8}A(1-\kappa_2)(\alpha^2-\beta^2)\sin 2\overline{\phi}_0 \tag{3.32}$$

or, finally,

$$\frac{d\overline{\phi}_0}{dt} = \tfrac{1}{2}\alpha\beta A^2 + \tfrac{1}{8}A(1-\kappa_2)(\alpha^2-\beta^2)\sin 2\overline{\phi}_0. \tag{3.33}$$

This controls the angle which $\overline{\phi}_0$ tends to, with

$$\sin 2\overline{\phi}_0 = -\frac{4A}{1-\kappa_2}\,\frac{\alpha\beta}{\alpha^2-\beta^2}\,. \tag{3.34}$$

Some care has to be taken, as the principal branch of the inverse sine function gives an unstable solution; the stable solutions lie in $\pi/2 \le \overline{\phi}_0 \le 3\pi/4$ modulo π, that is in the ranges N–NW or S–SE.

Once settled into the stable solution, the swimmer will swim in the $-\hat{\boldsymbol{\phi}}$ direction

$$\tilde{\boldsymbol{X}}_{\rm int} \simeq -(-\sin\overline{\phi}_0, \cos\overline{\phi}_0)\tilde{V}t, \quad \tilde{V} = \frac{8A^2\Lambda}{1-\kappa_2}\,\frac{\alpha\beta}{\alpha^2-\beta^2}\,, \tag{3.35}$$

that is $\overline{\phi}_0 - \pi/2$, E–NE or W–SW, noting that $\tilde{\boldsymbol{X}}_{\rm int}$ simplifies for small α_2 into the expression (3.6) used previously.

Figure 7 shows numerical results (solid) for the model $0{+}nH$, from solving (3.27–3.30) for three parameter sets. Dotted lines give asymptotic approximations. Panels (a,b,c) show results for parameter values in table 1, and there is a striking similarity with the simulations of the full model in figure 2: in particular compare the phase space in panels 2(c) and 7(b), and the direction and magnitude of motion in panels 2(f) and 7(c). The agreement in figure 7 with the asymptotic model (dotted) improves as the magnet becomes harder and $A_{\rm ext}$ is reduced, as should occur: in particular the system traverses the loop in phase space in a clockwise sense (negative area) and the swimmer moves in the $-\hat{\boldsymbol{\phi}}$ direction.

Note that for the values of table 1, in panel (c) the direction of the motion is poorly predicted by (3.35), but this is perhaps not surprising given the figure of eight motion in panel (b): this gives cancellations in the computation of the mean motion. Despite this (see rule of thumb 8 below), we give the following.

Rule of thumb 6: *when ϕ trapping occurs primarily through one magnet being nearly hard (the other remaining entirely soft) the swimmer orientation is N–NW or S–SE and it swims in the direction $-\hat{\boldsymbol{\phi}}$, namely E–NE or W–SW.*

Finally consider if we take model 0 and include both the effects of the varying moment of resistance and that of the nearly hard magnet to make a model $0{+}MoR{+}nH$, say. Within our perturbation theory the effects are additive at leading order, and we can see from combining (3.24) and (3.33) that in fact the effects tend to

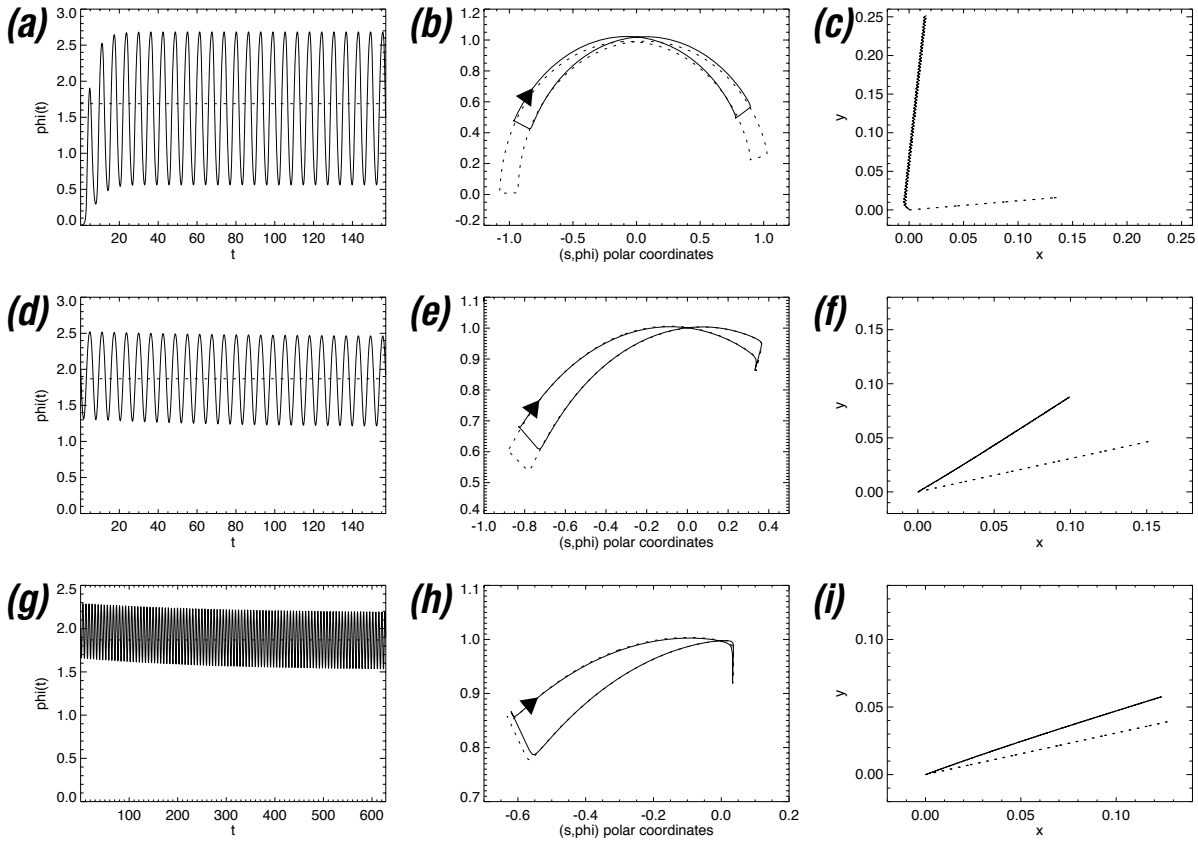

Fig. 7 Simulation of model 0+nH. In (a,d,g) we show $\phi(t)$ for (a,d) $0 \leq t \leq 25T$ or (g) $100T$, (b,e,h) limit cycle in phase space with (s, ϕ) polar coordinates, and (c,f,i) $\boldsymbol{X}_{\rm int}$ in the (x, y) plane for (c,f) $0 \leq t \leq 60T$ or (i) $100T$. In (a,b,c) parameters are as in table 1 but in (d,e,f) $A_{\rm ext} = 0.1$, $\kappa_2 = 0.9$ and in (g,h,i) $A_{\rm ext} = 0.05$ and $\kappa_2 = 0.95$.

cancel out and reduce the threshold for trapping (see rule of thumb 9 below). Pleasingly, this is exactly what we saw in figure 4 and confirms that going from figure 2 to 3 involves a transition between two quite distinct mechanisms for ϕ trapping.

3.5 *Model* 0+nS*: trapping for a nearly soft magnet*

The final mechanism we consider that can trap the angle ϕ for the swimmer, is to keep one magnet completely hard but replace the soft magnet by a general magnet. We thus set $\alpha_2 = 0$ but κ_1 has a general value and we

evolve α_1 by the equation (2.34) with $j = 1$. This is the 'not soft' or 'nearly soft' model, specified by

$$s = 1 - 2A_{\rm mag}\cos\alpha_1, \tag{3.36}$$

$$\dot{\phi} = Ab[\sigma^2\sin(\psi - \phi - \alpha_1) + \sin(\psi - \phi)], \tag{3.37}$$

$$\varsigma\varpi\,\dot{\alpha}_1 = (1 - \kappa_1)b\sin(\psi - \phi - \alpha_1) - \kappa_1\sin 2\alpha_1, \tag{3.38}$$

$$\tilde{\boldsymbol{X}}_{\rm int} = -\int_0^t 4\cos\alpha_1\,\dot{\phi}\,\hat{\boldsymbol{\phi}}\,dt, \tag{3.39}$$

and parameterised by A, the combination $\varsigma\varpi$, κ_1 and σ. We can investigate the nearly soft limit analytically. Assume that $\alpha_1 = \psi - \phi + a$ where $a(t) \ll 1$, $\kappa_1 \ll 1$ and take $\varsigma\varpi = 0$. The equation for the dipole direction yields

$$-b\sin a = \kappa_1\sin 2(\psi - \overline{\phi}_0). \tag{3.40}$$

From (3.37) we need to include a term on the right-hand side of (3.9) of the form $-A\sigma^2 b\sin a$, and this yields for the slow evolution of $\overline{\phi}_0$,

$$A^2\partial_\tau\overline{\phi}_0 = \Omega_0 + A\sigma^2\kappa_1\langle\sin 2(\psi - \overline{\phi}_0)\rangle. \tag{3.41}$$

A short calculation gives

$$\langle\sin 2(\psi - \overline{\phi}_0)\rangle = -\langle\cos^2\psi - \sin^2\psi\rangle\sin 2\overline{\phi}_0 = -\frac{\alpha - \beta}{\alpha + \beta}\sin 2\overline{\phi}_0, \tag{3.42}$$

and so we obtain

$$\frac{d\overline{\phi}_0}{dt} = \tfrac{1}{2}\alpha\beta A^2 - A\sigma^2\kappa_1\frac{\alpha - \beta}{\alpha + \beta}\sin 2\overline{\phi}_0. \tag{3.43}$$

Trapping occurs, with an angle given by

$$\sin 2\overline{\phi}_0 = \frac{\alpha\beta A}{2\sigma^2\kappa_1}\frac{\alpha + \beta}{\alpha - \beta}. \tag{3.44}$$

This will again swim with

$$\tilde{\boldsymbol{X}}_{\rm int} \simeq (-\sin\overline{\phi}_0, \cos\overline{\phi}_0)\tilde{V}t, \quad \tilde{V} = \frac{\alpha\beta A^2\Lambda}{\sigma^2\kappa_1}\frac{\alpha + \beta}{\alpha - \beta}. \tag{3.45}$$

Figure 8 shows numerical results (solid) for the $0{+}nS$ model for three parameter sets. As the softness of the magnet is increased, reading down the rows, the agreement with asymptotic results improves. However we can see that for the first row, the direction is predicted exactly wrongly by the asymptotic model! The reason is again in the cancellations in computing the average over the figure of eight loop in panel (b). In fact this loop shows a net negative signed area, whereas in the lower rows the area is positive. By rule of thumb 2 this corresponds precisely to the 180° change of direction we see going from row 1 to row 2. We will give a rule of thumb for this, followed by an obvious qualifying rule of thumb.

Rule of thumb 7: *when ϕ trapping occurs primarily through one magnet being nearly soft (the other remaining entirely hard) the swimmer orientation is given by the range E–NE or W–SW and it swims at an angle N–NW or S–SE.*

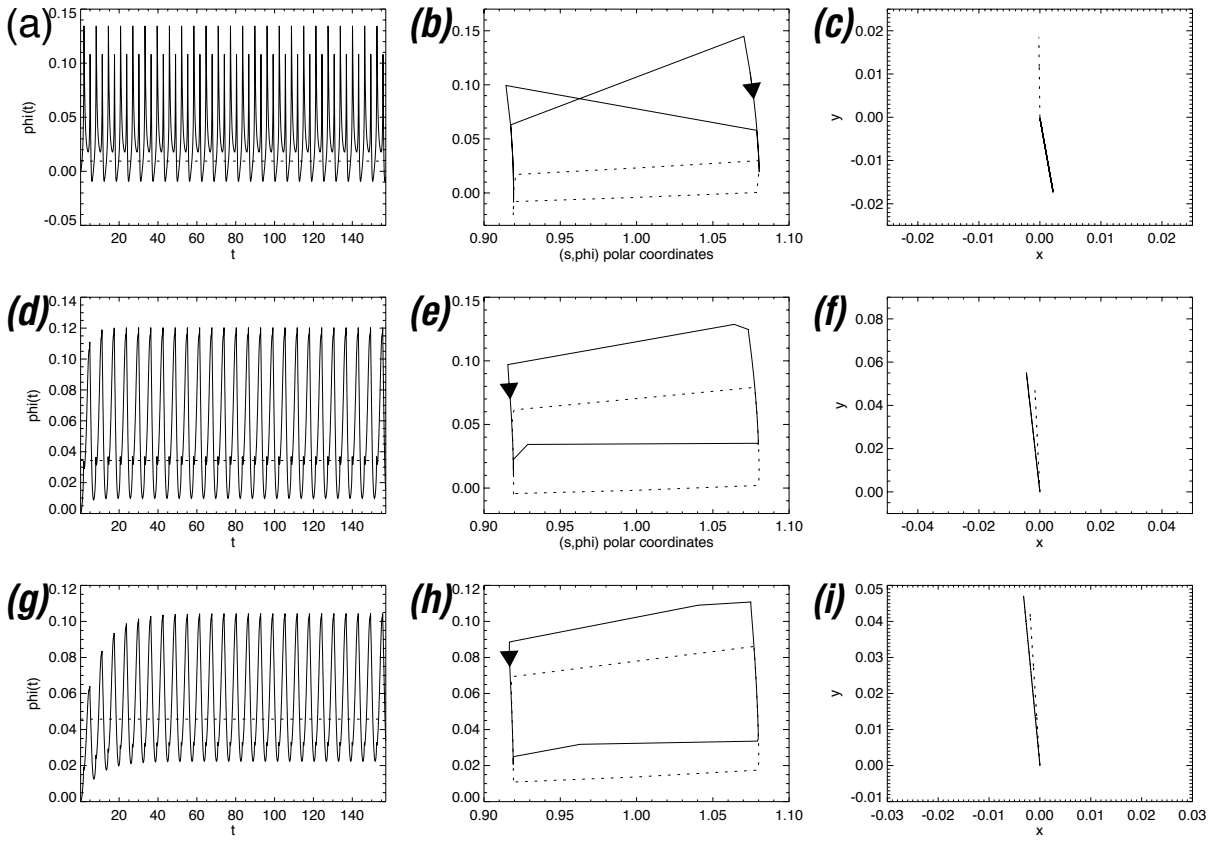

Fig. 8 Simulation of model $0{+}nS$, corresponding to $\kappa_2 = 1$. In (a,d,g) we show $\phi(t)$ for (a,d,g) $0 \le t \le 25T$, (b,e,h) limit cycle in phase space with (s, ϕ) polar coordinates, and (c,f,i) $\boldsymbol{X}_{\rm int}$ in the (x, y) plane for $0 \le t \le 100T$. In (a,b,c) parameters are as in table 1 but with $\kappa_1 = 0.1$. In (d,e,f) $A_{\rm ext} = 0.15$, $\kappa_1 = 0.02$ and in (g,h,i) $A_{\rm ext} = 0.1$ and $\kappa_2 = 0.01$.

Rule of thumb 8: *in a trapping regime where the limit cycle in the (s, ϕ) phase space shows a figure of eight form (so that there is significant cancellation in computing its signed area) rules of thumb 2, 3, 5, 6, 7 may well not work.*

Finally we observed above that the trapping mechanisms in models $0{+}MoR$ and $0{+}nH$ tend to cancel each other out, to reduce any threshold. For the $0{+}nS$ model, comparing (3.43) with (3.24) and (3.33), we obtain the following.

Rule of thumb 9: *the trapping effects of the moment of resistance (MoR) and a nearly soft magnet (nS) reinforce, to raise any threshold, while that for a nearly hard magnet (nH) is opposing.*

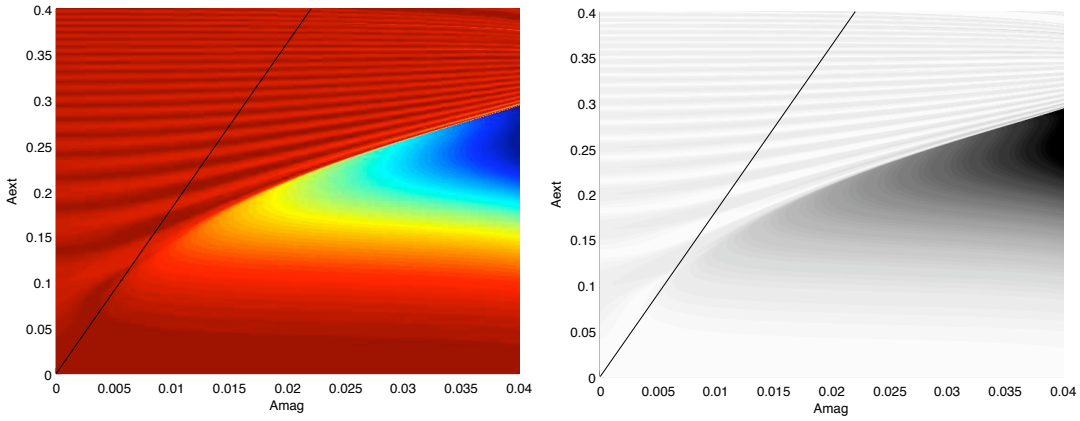

Fig. 9 Distance $\boldsymbol{X}_{\rm int}$ swum for the soft–hard model over a period $100T$, plotted in the $(A_{\rm mag}, A_{\rm ext})$ plane on a colour (black and white) scale from red (white) increasing to blue (black). The model $0{+}MoR$ threshold is shown. NOTE TO PUBLISHER/EDITOR: LEFT FIGURE IS FOR ONLINE VERSION, RIGHT FOR PRINTED VERSION. THE CAPTION IS THE SAME FOR BOTH.

4. Discussion

We have investigated the dynamics of a simple microscale swimmer based on two magnetised beads that are elastically connected and driven by an external magnetic field. The equations that were set up used a Lagrangian formulation for the dynamical parts, supplemented by equations for the direction of the magnetic dipoles of the beads: the decoupling of this magnetic evolution is justified, given that the dipole directions relax on a fast time scale, much shorter than hydrodynamic or dynamical effects.†

Within the resulting framework our numerical simulations identified the importance of 'trapping' the orientation ϕ of the swimmer, so that it does not simply move in a large-scale closed path. On the other hand we should note that motion in a closed path could be useful for micro-scale mixing and easy switching between different regimes could be valuable for applications. We then focussed on much simplified models and identified three effects that can lead to trapping and hence unidirectional motion. The first mechanism is the variation of the moment of resistance of the swimmer with the distance between the beads (one can think of a ballet dancer driven to spin in a viscous fluid). This leads to a threshold for trapping of the form

$$\frac{\alpha\beta A}{4\Lambda A_{\rm mag}} \equiv \frac{\alpha\beta A_{\rm ext}}{4\varpi\sigma\Lambda A_{\rm mag}} < 1 \tag{4.1}$$

(using (3.5)) and unidirectional swimming with velocity

$$\tilde{V} = \frac{\alpha\beta A^2}{2A_{\rm mag}} \equiv \frac{\alpha\beta A_{\rm ext}^2}{2\varpi^2\sigma^2 A_{\rm mag}}\,. \tag{4.2}$$

Note that $A_{\rm mag}$ is limited by (2.43): trapping then implies a limit on $A_{\rm ext}$ to be below the threshold and a

† An alternative model is to include the magnetic energies in the Lagrangian, leading to minor modifications to the equations for the angles α_j; see comments in [24].

consequent limit on the velocity. The above velocity $\tilde{V}$ can be linked to the velocity V in dimensionless units or the original dimensional velocity V^* by

$$V^* = l_0 \omega V, \quad V = \frac{3\varepsilon}{4} \frac{\chi_2 - \chi_1}{\rho + \rho^{-1}} A_{\mathrm{mag}} \tilde{V}. \tag{4.3}$$

To illustrate the usefulness and limitations of this theory, figure 9 shows a plot of the distance swum over a period $100T$ for the soft–hard system as in figure 3, in the $(A_{\mathrm{mag}}, A_{\mathrm{ext}})$ plane. There is a clear arced threshold above which motion is negligible and below which the distance travelled increases to a maximum. The mode $0{+}MoR$ threshold is the line shown and gives excellent agreement for small values of A_{ext} and A_{mag}; while incorrect for larger values, it clarifies the mechanism and the orders of magnitude involved.

The second and third trapping mechanisms involve the magnetic properties, and we focussed on cases where one magnet was completely hard or completely soft, to reduce the number of parameters of the problem. In each case we obtained thresholds for the trapping of the angle ϕ and corresponding velocities and directions of motion, with good agreement in the appropriate limit. These thresholds were obtained by asymptotic approximations valid in limits discussed above, and so should not be taken too seriously for firm quantitative estimates, but may be useful in qualitative comparison of effects and determination of different regimes in simulation and experiments. Similarly the rules of thumb above are a means by which we have tried to distil our work into useful information, but they are not hard and fast, and there will probably be subtleties we have missed, in particular when several effects may interact or in strongly nonlinear regimes. Indeed there are many other effects present in an experiment, such as drag and fluid interactions from the elastic filament and bending of the filament, and so our results should be taken only as indicative of regimes, mechanisms and scalings. A close comparison would require a computational fluid dynamics approach.

Note that we neglected inertia at an early point in our considerations, relevant to a Stokes regime. However there is also a short magnetic time scale in the problem and this does raise a question of whether inertia may always be neglected. In fact it is quite likely that in a situation where hysteresis gives rapid switching of the magnetic field on a short time scale inertia will not technically be negligible. On the other hand an instantaneous magnetic switching corresponds to a discontinuous force on the beads, and in a Stokes regime this would give a discontinuity in velocity but not in position. Inertial terms would come into play to smooth out such a discontinuity, but not contribute to motion. Our approximations were also based on ϖ being small, so that we neglected the fluid drag in the radial s direction to leave a purely elastic balance: increasing this parameter to moderate values is unlikely to change much in terms of qualitative behaviour, but if the parameter became large the above analysis would need to be revisited (for example for the case of two beads with negligible elastic coupling). The present work allows the possibility of many extensions, which are planned for future study, including motion in three dimensions, motion in a viscoelastic fluid, motion under other magnetic protocols (for example a Lissajou time dependence) and investigation of microscale stirring properties.

Acknowledgements

We are very grateful to Joe Griffiths of Paignton Community College for his work on the numerical side, in particular verifying theoretical thresholds, and to the Nuffield Foundation who supported his visit through a Science Bursary.

References

[1] Lighthill. M.J. 1969 Hydromechanics of aquatic animal propulsion. *Ann. Rev. Fluid Mech.* **1**, 413–446.

[2] Childress. S. 1981 *Mechanics of swimming and flying*. Cambridge University Press.

[3] Maxworthy, T. 1981 The fluid dynamics of insect flight. *Ann. Rev. Fluid Mech.* **13**, 329–350.

[4] Triantafyllou, M.S., Triantafyllou, G.S. & Yue, D.K.P. 2000 Hydrodynamics of fishlike swimming. *Ann. Rev. Fluid Mech.* **32**, 33–53.

[5] Wang, Z.J. 2005. Dissecting insect flight. *Ann. Rev. Fluid Mech.* **37**, 183–210.

[6] Purcell, E.M. 1977 Life at low Reynolds number. *Am. J. Phys.* **45**, 3–11.

[7] Lauga, E. & Powers, T.R. 2009 The hydrodynamics of swimming microorganisms. *Rep. Prog. Phys.* **72**, 096601.

[8] Najafi, A. & Golestanian, R. 2004 Simple swimmer at low Reynolds number: three linked spheres. *Phys. Rev. E* **69**, 062901.

[9] Earl, D.J., Pooley, C.M., Ryder, J.F., Bredberg, I. & Yeomans, J.M. 2007 Modeling microscopic swimmers at low Reynolds number. *J. Chem. Phys.* **126**, 064703.

[10] Golestanian, R. & Ajdari, A. 2008 Analytic results for the three-sphere swimmer at low Reynolds number. *Phys. Rev. E* **77**, 036308.

[11] Alexander, G.P., Pooley, C.M. & Yeomans, J.M. 2009 Hydrodynamics of linked sphere model swimmers. *J. Phys.: Condens. Matter* **21**, 204108.

[12] Alexander, G.P., Pooley, C.M. & Yeomans, J.M. 2008 Scattering of low Reynolds number swimmers. *Phys. Rev. E* **78**, 045302.

[13] Putz, V.B. & Yeomans, J.M. 2009 Hydrodynamic synchronisation of model microswimmers. *J. Stat. Phys.* **137**, 1001–1013.

[14] Felderholf, B.U. 2006 The swimming of animalcules. *Phys. Fluids* **18**, 063101.

[15] Friedman, G. 2007 Comment on 'The swimming of animalcules'. *Phys. Fluids* **19**, 079101.

[16] Felderholf, B.U. 2007 Response to "Coment on 'The swimming of animalcules' ". *Phys. Fluids* **19**, 079102.

[17] Biswal S.L., Gast A.P. 2004 Micromixing with linked chains of paramagnetic particles. *Anal Chem.* **76**. 6448–55.

[18] Dreyfus, R., Baudry, J., Roper, M.L., Fermigier, M., Stone, H.A. & Bibette, J. 2005 Microscopic articial swimmers. *Nature* **437**, 04090.

[19] Cēbers, A. & Javaitis, I. 2004 Dynamics of a flexible magnetic chain in a rotating magnetic field. *Phys. Rev. E* **69**, 021404.

[20] Gauger, E. & Stark, H. 2006 Numerical study of a microscopic artificial swimmer. *Phys. Rev. E* **74**, 021907.

[21] Keaveny, E.E. & Maxey, M.R. 2008 Spiral swimming of an articial micro-swimmer. *J. Fluid Mech.* **598**, 293–319.

[22] Ogrin, F.Y., Petrov, P.G. & Winlove, C.P. 2008 Ferromagnetic microswimmers. *Phys. Rev. Lett.* **100**, 218102.

[23] Happel, J. & Brenner, H. 1983 *Low Reynolds number hydrodynamics*. Kluwer, Dordrecht.

[24] Vilfan, A. & Stark, H. 2009 Comment on "Ferromagnetic microswimmers". *Phys. Rev. Lett.* **103**, 199801.

[25] Ogrin, F.Y., Petrov, P.G. & Winlove, C.P. 2009 Reply to "Comment on ferromagnetic microswimmers". *Phys. Rev. Lett.* **103**, 199802.

[26] Landau, L.D. & Lifshitz, E.M. 1959 *Fluid mechanics*. Butterworth–Heinemann.

[27] Abramowitz, M. & Stegun, I.A. 1972 *Handbook of mathematical functions*. Dover Publications.